Neural Comput & Applic (2017) 28:3725–3736
DOI 10.1007/s00521-016-2260-5

ORIGINAL ARTICLE

Adaptive robust finite-time neural control of uncertain PMSM servo system with nonlinear dead zone

Qiang Chen[1] · Xuemei Ren[2] · Jing Na[3] · Dongdong Zheng[2]

Received: 5 February 2015 / Accepted: 2 March 2016 / Published online: 19 March 2016

Abstract In this paper, an adaptive robust finite-time neural control scheme is proposed for uncertain permanent magnet synchronous motor servo system with nonlinear dead-zone input. According to the differential mean value theorem, the dead zone is represented as a linear time-varying system, and the model uncertainty including the dead zone is approximated by using a simple neural network. Then, an adaptive finite-time controller is designed based on a fast terminal sliding mode control principle, and the singularity problem in the initial TSMC is circumvented by modifying the terminal sliding manifold. Comparative experiments are conducted to validate the effectiveness and superior performance of the proposed method.

Keywords Adaptive control · Finite-time control · Dead zone · Servo system · Neural network

1 Introduction

Over the past decades, permanent magnet synchronous motor (PMSM) has been widely studied in motion-control applications [1–3]. The mechanical connection between servo motors and mechanical devices produces nonsmooth nonlinear characteristics such as dead zone, friction, backlash and hysteresis [4–7]. As one of the most important nonsmooth nonlinearities in motor servo systems, the dead zone may lead to severe control deterioration or even instability [8]. To handle the systems with unknown dead zones, much research has been carried out for the compensation of the dead zones [9–15].

Sliding mode control (SMC) is regarded as one of the robust control techniques to deal with system uncertainties and bounded disturbances. By introducing a nonlinear term into the SMC design, a terminal sliding mode control (TSMC) scheme was developed and the finite-time stability could be achieved [16–18]. Compared with SMC, TSMC has some superior properties, such as better tracking precision, fast convergence, insensitivity to system uncertainties and external disturbances. However, the singularity may exist in the TSMC scheme due to the use of negative fractional power in the designs of both sliding mode surface and controller. To avoid the singularity problem, nonsingular terminal sliding mode control methods were proposed in [19, 20], and a fast TSMC, which combined the advantages of the TSMC and the traditional linear SMC, was proposed in [21].

In those approaches aforementioned, the system models are required to be known or partially known, which will block the direct application for the PMSM servo control system since both model uncertainties and nonlinear dead zones are usually unavoidable. In this regard, neural networks (NNs) have been successfully employed to handle system uncertainties and unknown nonlinearities [12–15, 22–24]. Recently, Wang et al. [25] presented an indirect TSMC scheme with NN approximation to control robotic manipulators with model uncertainties, and the finite-time stability was ultimately guaranteed. However, the impact of nonsmooth nonlinearities, e.g., dead zone, was not

✉ Qiang Chen
sdnjchq@zjut.edu.cn

[1] College of Information Engineering, Zhejiang University of Technology, Hangzhou 310023, People's Republic of China

[2] School of Automation, Beijing Institute of Technology, Beijing 100081, People's Republic of China

[3] Kunming University of Science and Technology, Kunming 650093, People's Republic of China

considered in the controller design. In [26], a similar control scheme was developed for the finite-time attitude tracking control of spacecrafts with control input constraints, where only simulation results were given in the paper.

This paper focuses on an adaptive robust finite-time neural-network control (ARFTNC) for PMSM servo system with model uncertainties and unknown nonlinear dead-zone input. The main contribution of this paper is to develop an alternative fast terminal sliding mode control (FTSMC), and the singularity problem in the TSMC approach [16, 17] is avoided by modifying the terminal sliding manifold. Moreover, finite-time stability in both the reaching phase and the sliding phase is guaranteed, and comparative experiments are conducted to validate the effectiveness and superior performance of the proposed method.

The rest of this paper is organized as follows. The problem formulation and some preliminaries are briefly described in Sect. 2. Section 3 proposes an adaptive robust finite-time neural control based on a fast terminal sliding mode principle and NN approximation. The finite-time stability analysis is given in Sect. 4, followed by the comparative experiments in Sect. 5, and conclusions are provided in Sect. 6.

2 Problem formulation and preliminaries

The mechanical dynamics of PMSM servo system can be described as [8]:

$$\begin{aligned} &m\ddot{x} + f^*(\bar{x},t) + d^*(\bar{x},t) = k_0^* u(t) \\ &y = x \end{aligned} \tag{1}$$

where $\bar{x} = [x, \dot{x}]^T \in R^2$, $u(t) \in R$, $y \in R$ are state variables, the control input to the motor and the output from the motor, respectively; x is the position, m is the inertia, k_0^* is a positive control gain (the force constant), $f^*(\bar{x},t)$ is the friction force; $d^*(\bar{x},t)$ represents a bounded disturbance generated by coupling and protective covers, measurement noises, power electronics disturbances and other uncertainties.

For notational convenience, system (1) is normalized as:

$$\begin{aligned} &\ddot{x} = -h(\bar{x},t) + k_0 u(t) \\ &y = x \end{aligned} \tag{2}$$

where k_0 is a positive but unknown parameter satisfying $k_0 = k_0^*/m$; $h(\bar{x},t) = f(\bar{x},t) + d(\bar{x},t)$ with $f(\bar{x},t) = f^*(\bar{x},t)/m$ and $d(\bar{x},t) = d^*(\bar{x},t)/m$ being uncertain functions; the control input $u(t) \in R$ is the output of the following nonlinear dead zone shown in Fig. 1:

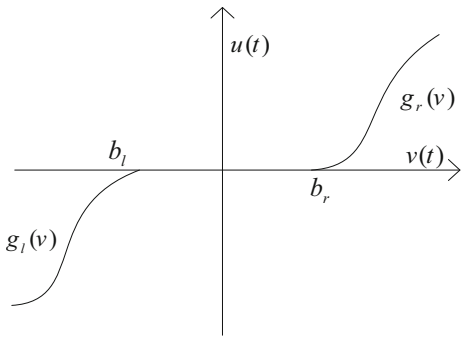

Fig. 1 Nonlinear dead-zone model

$$u(t) = G(v(t)) = \begin{cases} g_r(v(t)), & v(t) \geq b_r \\ 0, & b_l < v(t) < b_r \\ g_l(v(t)), & v(t) \leq b_l \end{cases} \tag{3}$$

where $v(t) \in R$ is the input of the dead zone (practical control signal), $g_l(v(t))$, $g_r(v(t))$ are unknown nonlinear smooth functions and b_l, b_r are unknown width parameters of the dead zone. Without loss of generality, we assume $b_l < 0$ and $b_r > 0$.

Remark 1 Although the dead-zone dynamics can be compensated in terms of its inverse model, the precise dead-zone model should be identified a priori. However, the maximum and minimum slope values of the dead zone are difficult to obtain practically, so the nonlinear dead zone (3) cannot be efficiently compensated by using identification techniques. In this paper, a model-independent compensation method is developed, in which the functions $g_l(v(t))$, $g_r(v(t))$ and characteristic parameters b_l, b_r are not necessarily known in prior.

To facilitate the controller design, the following assumption is needed.

Assumption 1 [13–15]: The functions $g_l(v(t))$ and $g_r(v(t))$ are smooth, and there exist unknown positive constants g_{l0}, g_{l1}, g_{r0} and g_{r1} such that

$$0 < g_{l0} \leq g_l'(v(t)) \leq g_{l1} \quad \forall v(t) \in (-\infty, b_l) \tag{4}$$

$$0 < g_{r0} \leq g_r'(v(t)) \leq g_{r1} \quad \forall v(t) \in (b_r, +\infty) \tag{5}$$

where $g_r(b_r) = g_l(b_l) = 0$, $g_l'(v(t)) = dg_l(z)/dz|_{z=v(t)}$ and $g_r'(v(t)) = dg_r(z)/dz|_{z=v(t)}$.

According to the differential mean value theorem and following the idea of [15], (3) can be rewritten as:

$$u(t) = \varphi(v(t))v(t) + \rho(v(t)) \quad \forall t \geq 0 \tag{6}$$

and

$$\varphi(v(t)) = \varphi_r(v(t)) + \varphi_l(v(t)) \tag{7}$$

where

$$\varphi_r(v(t)) = \begin{cases} g_r'(\xi_r), & v(t) > b_r \\ 0, & v(t) \le b_r \end{cases} \tag{8}$$

$$\varphi_l(v(t)) = \begin{cases} g_l'(\xi_l), & v(t) < b_l \\ 0, & v(t) \ge b_l \end{cases} \tag{9}$$

$$\rho(v(t)) = \begin{cases} -g_r'(\xi_r)b_r, & v(t) \ge b_r \\ -[g_l'(\xi_l) + g_r'(\xi_r)]v(t), & b_l < v(t) < b_r \\ -g_l'(\xi_l)b_l, & v(t) \le b_l \end{cases} \tag{10}$$

with $\xi_l \in (b_l, v(t))$ and $\xi_r \in (v(t), b_r)$.

Substituting (6) in (2), we have

$$\begin{aligned} \ddot{x} &= -h(\bar{x}, t) + k_0(\varphi(v(t))v(t) + \rho(v(t))) \\ y &= x. \end{aligned} \tag{11}$$

From Assumption 1, we can verify that $\varphi(v(t)) \in [\varphi_0, \varphi_1] \subset (0, +\infty)$ with $\varphi_0 = \min(g_{l0}, g_{r0})$ and $\varphi_1 = g_{l1} + g_{r1}$, $|\rho(v(t))| \le \rho_N$ with $\rho_N = (g_{l1} + g_{r1}) \max\{b_r, -b_l\}$ being a positive constant.

Remark 2 The reformulation of dead-zone dynamics was inspired by [14, 15]. However, the tracking error is proved to be semiglobally uniformly ultimately bounded in the former works and only simulation results are provided. In this paper, the tracking error e can be controlled to converge to the equilibrium point within a finite time, which leads to improved experiment results.

Let y_d be a given twice differentiable desired trajectory and then the tracking error e is defined as

$$e = y_d - y. \tag{12}$$

The control objective is to design an adaptive robust finite-time controller $v(t)$ for the system (11) such that the tracking error e converges to the equilibrium point within a finite time, while all signals in the closed-loop system are bounded.

3 Adaptive robust finite-time control

In this section, an adaptive robust finite-time control scheme is designed for the PMSM servo system (11).

3.1 Fast terminal sliding manifold

The linear sliding mode (LSM) and terminal sliding mode (TSM) can be formulated by the following differential equations [25, 27]:

LSM:

$$s = \dot{e} + \lambda_0 e \tag{13}$$

TSM:

$$s = \dot{e} + \lambda_0 |e|^{\gamma} \mathrm{sgn}(e). \tag{14}$$

where $\lambda_0 > 0$, and $\gamma = q/p$, $p, q > 0$ are positive odd numbers satisfying $q < p$.

Remark 3 Once the sliding mode manifold $s = 0$ is reached, the expressions of LSM and TSM become $\dot{e} = -\lambda_0 e$ and $\dot{e} = -\lambda_0 |e|^{\gamma} \mathrm{sgn}(e)$, respectively. Since $0 < \gamma < 1$, $|e|^{\gamma} < |e|$ if $|e| > 1$, which implies that TSM has a slower convergence speed than LSM when the system position is far away from the desired trajectory. Otherwise, when the system position is close to the desired trajectory, TSM has a faster convergence speed than LSM due to $|e|^{\gamma} > |e|$ if $|e| < 1$.

By introducing the linear term of (13) into the TSM design (14), a fast terminal sliding mode (FTSM) is defined as:

$$\begin{aligned} s &= \dot{e} + \lambda_1 e + \lambda_2 |e|^{\gamma} \mathrm{sgn}(e) \\ &= x_r - \dot{x} \end{aligned} \tag{15}$$

with

$$x_r = \dot{y}_d + \lambda_1 e + \lambda_2 |e|^{\gamma} \mathrm{sgn}(e) \tag{16}$$

where $e \in R$, $\lambda_1, \lambda_2 > 0$, $\gamma = q/p$, $p, q > 0$ are positive odd numbers satisfying $q < p$.

Then, the derivative of s is

$$\dot{s} = \dot{x}_r - \ddot{x} \tag{17}$$

with

$$\dot{x}_r = \ddot{y}_d + \lambda_1 \dot{e} + \lambda_2 \gamma |e|^{\gamma - 1} \dot{e}. \tag{18}$$

Remark 4 Compared with the term $x^{p/q}$ used in [25, 26], we employ the term $|e|^{\gamma} \mathrm{sgn}(e)$ in this paper to design the sliding mode and the controller. This modification is significant for the practical experiment because the fractional power $\gamma = q/p$ may result in the term $e^{\gamma} \notin R$ and thus $\dot{e} \notin R$ for $e < 0$. In that case, the control signal $v \notin R$ will contain the imaginary part and may lead to control deterioration or even trigger instability.

On the sliding mode surface $s = 0$, (15) can be rewritten as

$$\dot{e} = -\lambda_1 e - \lambda_2 |e|^{\gamma} \mathrm{sgn}(e) \tag{19}$$

According to the finite-time stability theory [28], the equilibrium point $e = 0$ of differential equation (19) is finite-time stable; i.e., the tracking error can converge to the equilibrium point within a finite settling time

$$T = \frac{1}{\lambda_1 (1 - \gamma)} \ln \frac{\lambda_1 |e_0|^{1 - \gamma} + \lambda_2}{\lambda_2}. \tag{20}$$

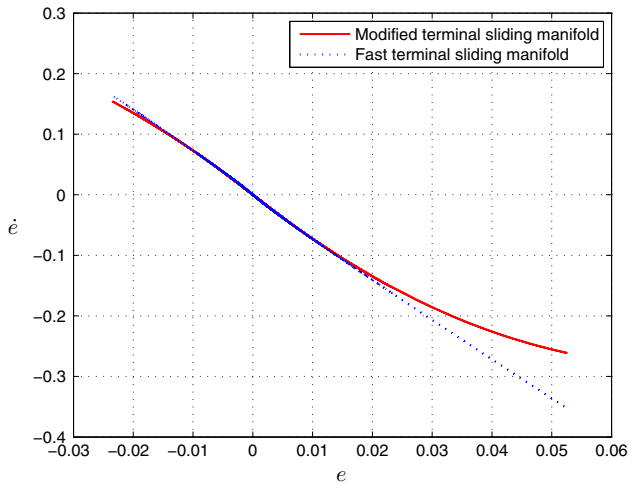

Fig. 2 Modified terminal sliding manifold

Substituting (19) in (18), we have

$$\begin{aligned}\dot{x}_r &= \ddot{y}_d + \lambda_1\dot{e} + \lambda_2\gamma|e|^{\gamma-1}\dot{e} \\ &= \ddot{y}_d - \lambda_1^2 e - \lambda_1\lambda_2(\gamma+1)|e|^{\gamma}\mathrm{sgn}(e) - \lambda_2^2\gamma|e|^{2\gamma-1}\mathrm{sgn}(e).\end{aligned} \tag{21}$$

It should be noted that if $\gamma > 1/2$, the singularity of (21) will not occur since there is no negative fractional power in $\ddot{x}_r$. However, in case that $s \neq 0$ and $e = 0$, the singularity still exists. Motivated by the work of [25, 26], the singularity problem is avoided by modifying the definition of x_r as

$$x_r = \dot{y}_d + \lambda_1 e + \lambda_2\beta(e) \tag{22}$$

where

$$\beta(e) = \begin{cases} |e|^{\gamma}\mathrm{sgn}(e) & s = 0 \text{ or } s \neq 0, |e| > \mu \\ l_1 e + l_2|e|^2\mathrm{sgn}(e) & s \neq 0, |e| \leq \mu \end{cases} \tag{23}$$

with $l_1 = (2-\gamma)\mu^{\gamma-1}$, $l_2 = (\gamma-1)\mu^{\gamma-2}$, $\mu > 0$ being a small positive constant.

Then, the derivative of x_r is obtained as

$$\dot{x}_r = \begin{cases} \ddot{y}_d + \lambda_1\dot{e} + \lambda_2\gamma|e|^{\gamma-1}\dot{e}, & s = 0 \text{ or } s \neq 0, |e| \geq \mu \\ \ddot{y}_d + \lambda_1\dot{e} + \lambda_2 l_1\dot{e} + 2\lambda_2 l_2|e|\dot{e}, & s \neq 0, |e| \leq \mu \end{cases} \tag{24}$$

which is a continuous function. Therefore, compared with (21), there exists no singularity problem in Eq. (24).

From (14), (22) and (23), the modified terminal sliding manifold as shown in Fig. 2 is expressed as

$$s = \dot{e} + \lambda_1 e + \lambda_2\beta(e). \tag{25}$$

From (11) and (24), the derivative of s is obtained as:

$$\dot{s} = -k_0\varphi(v(t))v(t) + \kappa(t) \tag{26}$$

where $\kappa(t)$ is a nonlinear function and expressed as

$$\kappa(t) = \dot{x}_r + h(\bar{x}, t) - k_0\rho(v(t)). \tag{27}$$

Since k_0, $\varphi(v(t))$ and $\kappa(t)$ are unknown, the neural network (NN) in [15] is employed to approximate a nonlinear function $H = \kappa(t)/(k_0\varphi(v(t)))$ due to its inherent approximation capabilities. Then, the function H can be expressed as

$$H = W^{*T}\phi(X) + \varepsilon \tag{28}$$

where $X = [x^T, \dot{x}^T, y_d^T, \dot{y}_d^T, \ddot{y}_d^T]^T \in R^5$ is the input vector; $W^* = [w_1, w_2, \ldots, w_5]^T \in R^5$ is the ideal bounded weight matrix and ε is the bounded approximation error, which satisfy $\|W^*\| \leq W_N$ and $|\varepsilon| \leq \varepsilon_N$ with W_N and ε_N being positive constants, respectively; $\phi(X)$ represents the NN basis function.

Remark 5 The employed neural network is one of the linearly parameterized approximation methods and can be replaced by any other approximation approaches, such as RBF neural network, fuzzy systems. However, the structure of the employed neural network in this paper is simpler than the other neural networks. In the employed neural network, there is no hidden layer, but only five inputs and one output are included, such that the corresponding weight matrix is 5×1. Consequently, although consuming a little more time than PID approach, the proposed method is still easy to run in the DSP (TMS3202812)-based practical system.

Remark 6 From Assumption 1, we can obtain $\varphi(v(t)) \in [\varphi_0, \varphi_1]$ with k_0, $\varphi_0 = \min(g_{l0}, g_{r0})$ and $\varphi_1 = g_{l1} + g_{r1}$ being positive constants, so $k_0\varphi(v(t)) \neq 0$ is always guaranteed, and the function H can be approximated by NN without any singularity problem.

3.2 Controller design

In the following, an adaptive robust finite-time neural controller is developed for tracking control of the system (11).

The controller is designed as:

$$v(t) = \hat{W}^T\phi(X) + k_1 s + k_2|s|^r\mathrm{sgn}(s) + (\delta_1 + \delta_2)\mathrm{sgn}(s) \tag{29}$$

where $\hat{W}$ is the estimate of the ideal weight W^*, $\hat{W}^T\phi(X)$ is the NN uncertainty estimator, $k_1 s + k_2|s|^r\mathrm{sgn}(s)$ is a feedback control to guarantee the finite-time convergence of sliding mode s, $(\delta_1 + \delta_2)\mathrm{sgn}(s)$ is a robust term which is designed to provide robustness in the presence of the NN approximation and weight estimation errors. Here, $k_1 > 0$ and $k_2 > 0$ are the designed control parameters, $r = r_1/r_2$ with $r_1, r_2 > 0$ being positive odd numbers satisfying

$r_1 < r_2$, $\delta_1 > \varepsilon_N$, and δ_2 is a positive constant satisfying $\delta_2 > \|\tilde{W}^T\phi(X)\|_F$.

The weight update law is given by

$$\dot{\hat{W}} = \Gamma\phi(X)s \tag{30}$$

where Γ is a positive-definite and diagonal matrix; $\phi(X)$ is chosen as the following sigmoid function

$$\phi(X) = \frac{a}{b + e^{(-X/c)}} + d \tag{31}$$

with a, b, c and d being appropriate parameters.

Substituting the proposed controller (29) in (26), we have

$$\dot{s} = k_0\varphi(v(t))[\tilde{W}^T\phi(X) - k_1 s - k_2|s|^r\mathrm{sgn}(s) + \varepsilon - (\delta_1 + \delta_2)\mathrm{sgn}(s)] \tag{32}$$

where $\tilde{W} = W^* - \hat{W}$ is the NN weight estimation error.

Remark 7 Since the discontinuous switching function $\mathrm{sgn}(\cdot)$ shown in (29) and (32) may result in the chattering phenomenon, the following continuous function $\eta(\cdot)$ is employed instead in the experiment section:

$$\eta(s) = \begin{cases} \mathrm{sgn}(s) & |s| \geq \zeta \\ \dfrac{2s}{|s| + \zeta} & |s| < \zeta \end{cases} \tag{33}$$

where $\zeta > 0$ is a small positive number which represents the boundary layer thickness.

4 Stability analysis

In this section, a lemma and a theorem are provided to show the boundedness of all signals and the finite-time stability of system (11) in both the reaching phase and the sliding phase.

Lemma 1 [20] Suppose that there exists a continuous, positive-definite function $V(t)$ satisfying the following differential inequality:

$$\dot{V}(t) + \alpha V(t) + \beta V^{\gamma}(t) \leq 0, \quad \forall t \geq t_0, \quad V(t_0) \geq 0 \tag{34}$$

where $\alpha, \beta > 0$, $0 < \gamma < 1$ are constants. Then, for any given t_0, $V(t)$ satisfies the following inequality:

$$V^{1-\gamma}(t) \leq (\alpha V^{1-\gamma}(t_0) + \beta)e^{-\alpha(1-\gamma)(t-t_0)} - \beta, \quad t_0 \leq t \leq t_s \tag{35}$$

and

$$V(t) \equiv 0, \quad \forall t \geq t_s \tag{36}$$

with t_s given by

$$t_s = t_0 + \frac{1}{\alpha(1-\gamma)}\ln\frac{\alpha V^{1-\gamma}(t_0) + \beta}{\beta}. \tag{37}$$

Theorem 1 Consider the PMSM servo system (11) with unknown nonlinear dead zone (3), terminal sliding manifold (25), control law (29) and weight update law (30), then

1. All the signals of the closed-loop system are semiglobally uniformly ultimately bounded (SGUUB).
2. The terminal sliding manifold s can converge to the equilibrium point within a finite time if the design parameters δ_1 and δ_2 are chosen as $\delta_1 \geq \varepsilon_N$ and $\delta_2 \geq \|\tilde{W}^T\phi(X)\|_F$.
3. The tracking error e will converge to the equilibrium point within a finite time.

Proof

1. Choose the following Lyapunov function:

$$V(t) = \frac{1}{2k_0\varphi_0}s^2 + \frac{1}{2}\tilde{W}^T\Gamma^{-1}\tilde{W}. \tag{38}$$

Differentiating (38) with respect to time and using (32) yield

$$\begin{aligned}\dot{V}(t) &= \frac{1}{k_0\varphi_0}s\dot{s} + \tilde{W}^T\Gamma^{-1}\dot{\tilde{W}} \\ &\leq \tilde{W}^T\phi(X)s - (\delta_1 + \delta_2)|s| - k_1 s^2 - k_2|s|^{r+1} + |s|\varepsilon \\ &\quad - \tilde{W}^T\Gamma^{-1}\dot{\hat{W}} \\ &= -\tilde{W}^T\Gamma^{-1}[\dot{\hat{W}} - \Gamma\phi(X)s] - (\delta_1 + \delta_2)|s| + |s|\varepsilon \\ &\quad - k_1 s^2 - k_2|s|^{r+1}.\end{aligned} \tag{39}$$

Substituting (30) in (39), we have

$$\dot{V}(t) \leq -k_1 s^2 - k_2|s|^{r+1} - \delta_2|s| \leq 0. \tag{40}$$

Because the NN approximation is feasible in a compact set, the resulting stability will be proved in semiglobal sense. From (38) to (40), we can conclude that both s and $\tilde{W}$ are semiglobally uniformly ultimately bounded. Considering (15) and the boundedness of W^*, it can be obtained that both e, $\dot{e}$ and $\hat{W}$ are also semiglobally uniformly ultimately bounded, and thus, $v(t)$ is bounded according to (29). Since y_d, $\dot{y}_d$ and $\ddot{y}_d$ are bounded, the boundedness of x_r and $\dot{x}_r$ is guaranteed by (16) and (18). From (32), it can be concluded that $\dot{s}$ is semiglobally uniformly ultimately bounded due to the boundedness of $\varphi(v(t))$. Therefore, all signals of the closed-loop system are semiglobally uniformly ultimately bounded.

2. From (31), we can conclude that the sigmoid function $\phi_i(X)$ is bounded by $0 < \phi_i(X) < L_0$, $i = 1, \ldots, L_1$, with $L_0 = \max\{|\frac{a}{b} + d|, |\frac{a}{b+1} + d|\}$. Therefore, $\phi(X)$ is bounded by

$$\|\phi(X)\| \le L_0\sqrt{L_1} \tag{41}$$

where $\|.\|$ denotes the Euclidean norm of a vector, $\phi(X) = [\phi_1(X), \ldots, \phi_L(X)]^T$.
According to the property of Frobenius norm, we can obtain

$$\|\tilde{W}^T\phi(X)\|_F \le \|\tilde{W}\|_F\|\phi(X)\|. \tag{42}$$

Select a Lyapunov function candidate

$$V_1 = \frac{1}{2k_0\varphi_0}s^2. \tag{43}$$

Differentiating (43) and using (32), we have

$$\begin{aligned}\dot{V}_1 &= \frac{1}{k_0\varphi_0}sk_0\varphi(v(t))[\tilde{W}^T\phi(X) + \varepsilon - k_1 s - k_2|s|^r\mathrm{sgn}(s) \\ &\quad - (\delta_1 + \delta_2)\mathrm{sgn}(s)] \\ &\le -k_1 s^2 - k_2|s|^{r+1} + \|\tilde{W}^T\phi(X)\|_F|s| + |s|\varepsilon \\ &\quad - (\delta_1 + \delta_2)|s|.\end{aligned} \tag{44}$$

Since $\delta_1 \ge \varepsilon_N$ and $\delta_2 \ge \|\tilde{W}^T\phi(X)\|_F$, (44) is rewritten as

$$\begin{aligned}\dot{V}_1 &\le -k_1 s^2 - k_2|s|^{r+1} \\ &\le -2k_1k_0\varphi_0\left(\frac{1}{2}\frac{1}{k_0\varphi_0}s^2\right) - k_2(2k_0\varphi_0)^{\frac{r+1}{2}}\left(\frac{1}{2}\frac{1}{k_0\varphi(v(t))}s^2\right)^{\frac{r+1}{2}} \\ &= -\bar{k}_1 V_1 - \bar{k}_2 V_1^{\bar{k}_3}.\end{aligned} \tag{45}$$

Then, we can obtain

$$\dot{V}_1 + \bar{k}_1 V_1 + \bar{k}_2 V_1^{\bar{k}_3} \le 0 \tag{46}$$

where $\bar{k}_1 = 2k_1k_0\varphi_0$, $\bar{k}_2 = k_1(2k_0\varphi_0)^{\frac{r+1}{2}}$ and $\bar{k}_3 = \frac{r+1}{2}$.
According to Lemma 1, it can be concluded that the fast terminal sliding manifold s can converge to the equilibrium point within a finite time t_1 given by

$$t_1 = \frac{1}{\bar{k}_1(1-\bar{k}_3)}\ln\frac{\bar{k}_1 V_1^{1-\bar{k}_3}(t_0) + \bar{k}_2}{\bar{k}_2}. \tag{47}$$

From (47), we can see that the reaching time t_1 is independent of the error dynamics of system (11) but depends on the constant k_0, k_1 and φ_0 only.

3. Once the sliding surface $s = 0$ is achieved, the states of system (11) will remain on it and the system has the invariant properties. On the sliding surface $s = 0$, we can obtain

$$\dot{e} = -\lambda_1 e - \lambda_2|e|^{\gamma}\mathrm{sgn}(e). \tag{48}$$

Constructing the following Lyapunov candidate

$$V_2 = \frac{1}{2}e^2 \tag{49}$$

and differentiating V_2 along (48) yields:

$$\begin{aligned}\dot{V}_2 &= -\lambda_1 e^2 - \lambda_2|e|^{\gamma+1} \\ &= -2\lambda_1 V_2 - \lambda_2 2^{\frac{\gamma+1}{2}}V_2^{\frac{\gamma+1}{2}}.\end{aligned} \tag{50}$$

Setting $\beta_1 = 2\lambda_1$, $\beta_2 = \lambda_2 2^{\frac{\gamma+1}{2}}$ and $\beta_3 = \frac{\gamma+1}{2}$, it can be obtained from (50) as

$$\dot{V}_2 + \beta_1 V_2 + \beta_2 V_2^{\beta_3} \le 0. \tag{51}$$

According to Lemma 1, we can conclude that the tracking error e will converge to the equilibrium point within a finite time t_2 given by

$$t_2 = \frac{1}{\beta_1(1-\beta_3)}\ln\frac{\beta_1 V_2^{1-\beta_3}(t_0) + \beta_2}{\beta_2}. \tag{52}$$

□

Remark 8 The nonsingular terminal sliding mode control (NTSMC) scheme in Ref. [20] is a kind of discontinuous boundary layer approach to deal with the singularity problem, and the time taken to reach the terminal sliding mode depends on the error dynamics of the mechanical system. But in this paper, we present a continuous nonsingular terminal sliding mode control, and according to (47) and (52), we can see that the reaching time t_1 and t_2 are both independent of the error dynamics, but only related to the constant parameters, i.e., $\bar{k}_i$ and β_i, respectively.

Remark 9 From (47) and (52), it can be concluded that in order to reduce the reaching time t_1 and t_2, we need to increase the value of parameters k_1, λ_1, r and γ. However, too large k_1 and λ_1 may lead to a high gain of the controller (29). Consequently, we should choose the proper value of parameters k_1 and λ_1, and sufficiently large value of r and γ.

5 Experimental results

5.1 Description of the experimental test-rig

As shown in Fig. 3, a turntable servo system with one degree of freedom (DOF) is used as the test-rig to validate the proposed control, which comprises a permanent magnet synchronous motor (PMSM, HC-UFS13), an encoder and pulse width modulation (PWM) amplifiers in the motor drive card (MR-J2S-10A), a digital signal processing unit (DSP, TMS3202812) performing as the controller and a Pentium 2.8-GHz PC operating for display. The proposed tracking control algorithm is implemented by a C-program in CCS3.0 programming

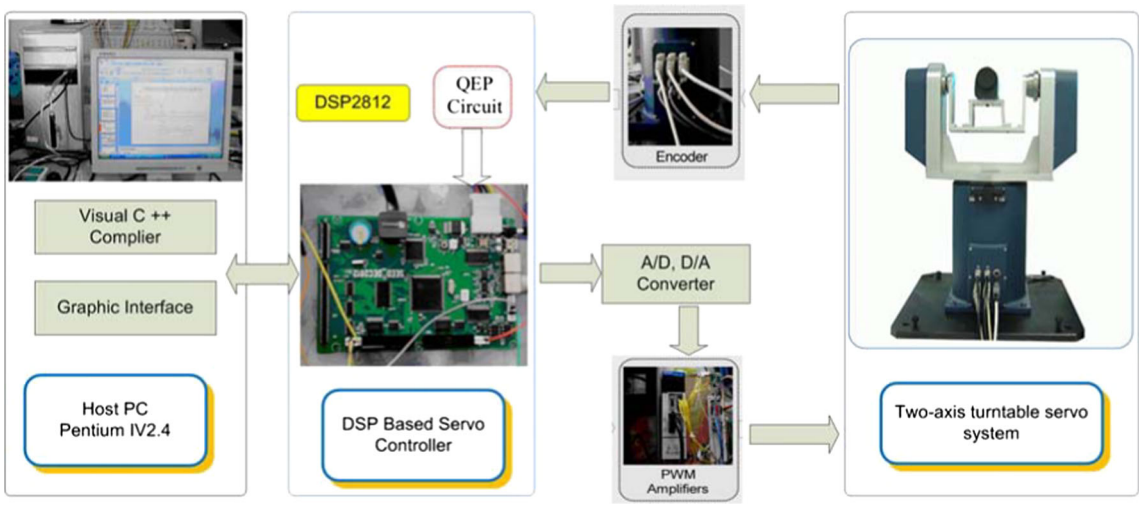

Fig. 3 Turntable PMSM servo system

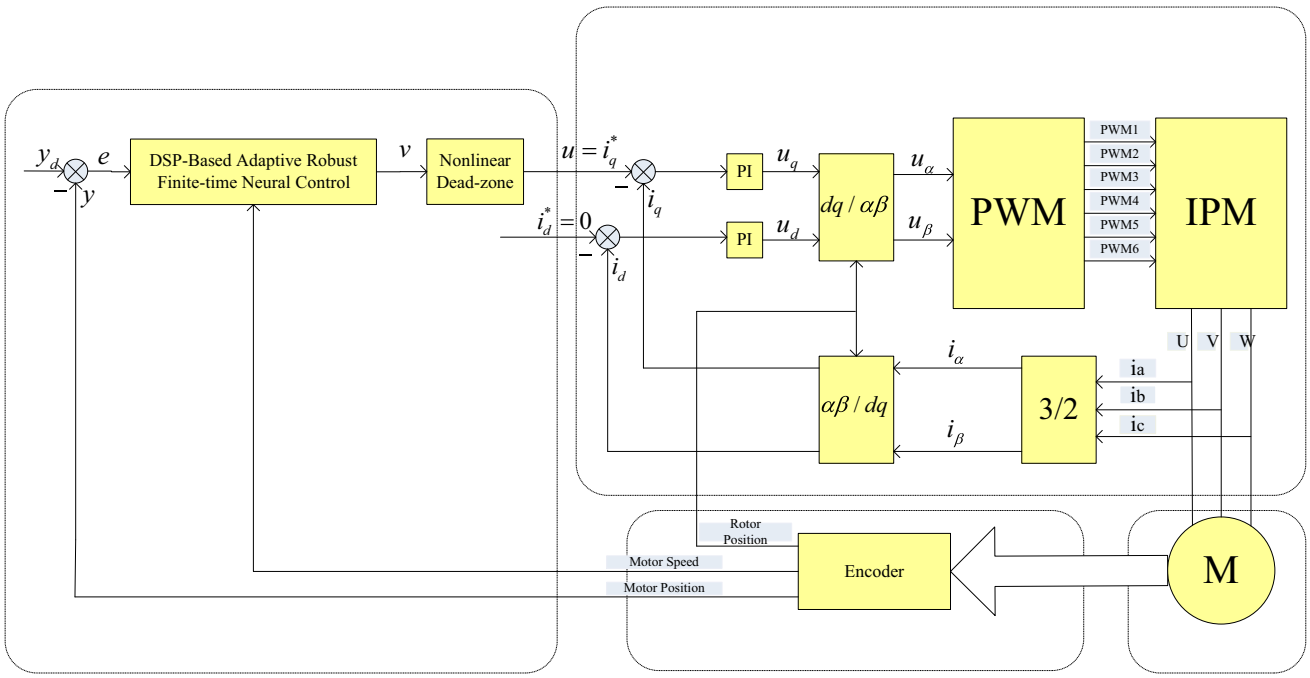

Fig. 4 Schematic diagram of the proposed control system

environment. The total run time is 20 s with the sampling time selected as 0.01 s. The schematic diagram of the proposed control system is depicted by Fig. 4. The PMSM is driven by a PWM voltage source inverter, and the i_d and i_q control loops are controlled by two identical PI controllers which make the current transients negligible with respect to the mechanical dynamics (i.e., $i_d^* = i_d = 0$ and $i_q^* = i_q = u(t)$ where superscript '*' denotes reference signals and u indicates controller output).

5.2 Design of controllers

In this section, extensive experiments are conducted on the turntable PMSM servo system. In order to show the superior tracking performance of the proposed scheme, four different control schemes, including adaptive robust finite-time neural control (ARFTNC), NN-based terminal sliding mode control (NNTSMC) [25], NN-based linear sliding mode control (NNLSMC) [27] and PID control,

are performed in the experiments. It should be noted that in NNTSMC and NNLSMC, NN is employed to approximate the unknown nonlinearities, while the compensation for the dead-zone dynamics is not considered. For fair comparison, the initial states of the system and NN parameters are set the same, i.e., $(x(0), \dot{x}(0)) = (0, 0)$, $\Gamma = 0.05$, $a = 2$, $b = 10$, $c = 1$ and $d = -10$.

5.2.1 Adaptive robust finite-time neural control (ARFTNC)

In the proposed control scheme, the fast terminal sliding manifold is selected as (25), where the parameters are set as $\gamma = 9/11$, $\lambda_1 = 5$ and $\lambda_2 = 1$. The designed controller is given by (29), and the control parameters are $k_1 = 0.5$, $k_2 = 0.1$, $r = 9/11$, $\delta_1 = \delta_2 = 0.01$ and $\zeta = 0.001$.

5.2.2 NN-based terminal sliding mode control (NNTSMC)

In this scheme, the terminal sliding manifold is defined as (14), where $\gamma = 9/11$, $\lambda_0 = 6$. The controller is addressed as

$$v(t) = \hat{W}^T \phi(X) + k_0 |s|^r \mathrm{sgn}(s) + (\delta_1 + \delta_2)\mathrm{sgn}(s) \tag{53}$$

where $k_0 = 0.6$, $r = 9/11$, $\delta_1 = \delta_2 = 0.01$ and $\zeta = 0.001$.

5.2.3 NN-based linear sliding mode control (NNLSMC)

In this scheme, the linear sliding manifold is chosen as (13), where $\lambda_0 = 6$. The controller is expressed as

$$v(t) = \hat{W}^T \phi(X) + k_0 s + (\delta_1 + \delta_2)\mathrm{sgn}(s) \tag{54}$$

where $k_0 = 0.6$, $\delta_1 = \delta_2 = 0.01$ and $\zeta = 0.001$.

5.2.4 PID control

In the PID controller, the control parameters $k_P = 40$, $k_D = 40$ and $k_I = 0.05$ are determined by using a heuristic tuning approach for a given reference signal, e.g., $y_d = 0.6\sin(2\pi t/5)$.

5.3 Comparative results

The following four indices are adopted to compare the tracking performance of each control algorithm.

1. IAE = $\int |e(t)|\mathrm{d}t$, which is the integrated absolute error to measure the system tracking performance.
2. ISDE = $\int (e(t) - e_0)^2 \mathrm{d}t$, which is the integrated square error and used to demonstrate the smoothness of the profile.
3. IAU = $\int |u(t)|\mathrm{d}t$, which is the integrated absolute control and taken as a measurement of the overall amount of control effort.
4. ISDU = $\int (u(t) - u_0)^2 \mathrm{d}t$, which is the integrated square control and used as a measurement of the fluctuations of control signal around its mean value.

Then, three experimental examples are performed for the fair comparison of four different controllers. It is noted that in the practical tests, there are unavoidable disturbances and unknown dynamics. Hence, the robustness and disturbance rejection of the controllers can be evaluated in terms of above indices.

5.3.1 Example I: Tracking control of a specified sinusoidal wave

In the first experimental example, the reference trajectory is specified as $y_d = 0.6\sin(2\pi t/5)$, and the comparative tracking control performances of four different controllers are shown in Fig. 5. Figure 5a depicts the whole tracking performance of the different control schemes, while Fig. 5b, c provides the corresponding tracking errors and control signals, respectively. From Fig. 5, we can see that the proposed ARFTNC method can provide better tracking performance than that of other three controllers (i.e., convergence speed, steady-state errors). In particular, the proposed ARFTNC can obtain faster convergence speed than NNTSMC because of the linear term $k_1 s$ in the sliding manifold, and ARFTNC can achieve smaller tracking error than NNLSMC due to the terminal sliding mode term $k_2|s|^r\mathrm{sgn}(s)$.

In order to compare the control performance, the experimental results in terms of performance indices are given by Table 1. From the table, we can obtain that the proposed ARFTNC scheme has the smallest IAE, ISDE and ISDU, which means it performs best among four controllers. PID controller gives the largest IAE, ISDE and IAU, which implies the poorest tracking performance among four controllers. The NNLSMC and NNTSMC achieve similar ultimate tracking performance in terms of IAE and ISDE. However, NNLSMC requires a relatively greater control effort (i.e., IAU), while NNTSMC provides a relatively larger fluctuations (i.e., ISDU).

5.3.2 Example II: Tracking control of sinusoidal waves with varying amplitudes

In order to demonstrate better tracking performance of the proposed method among wide operation conditions, we choose a sinusoidal signal $y_d = A\sin(2\pi t/5)$ with a fixed period $T = 5$ s and varying amplitudes $A = 0.4 \sim 1.2$ rad as

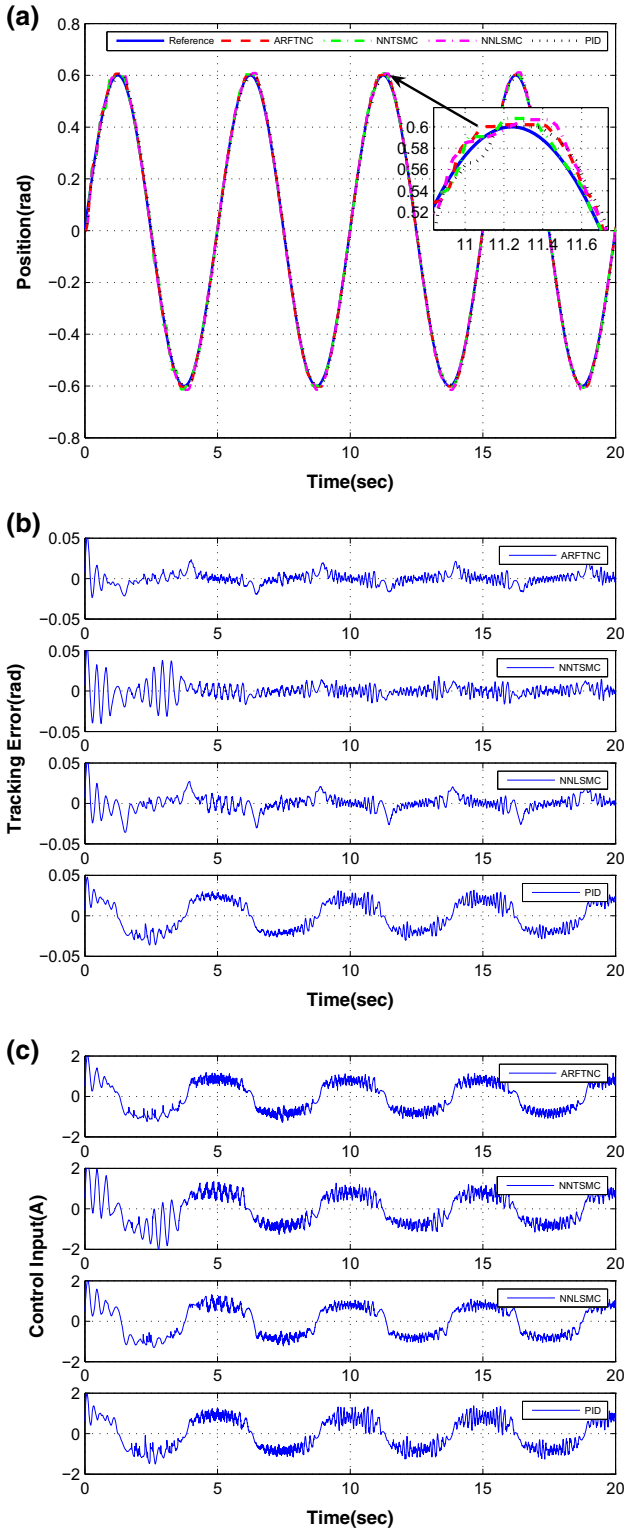

Fig. 5 Tracking control performance for $y_d = 0.6\sin(2\pi/5)$. **a** Tracking trajectories of four different controllers. **b** Tracking errors of four different controllers. **c** Control signals of four different controllers

Table 1 Comparison for sinusoid reference for $y_d = 0.6\sin(2\pi t/5)$

	PID	NNLSMC	NNTSMC	ARFTNC
IAE	0.3837	0.1393	0.1341	0.1228
ISDE	0.0072	0.0020	0.0020	0.0015
IAU	14.2714	14.1097	13.6765	13.8337
ISDU	11.9107	11.3043	11.9163	11.1005

Table 2 Tracking control performance IAE for $y_d = A\sin(2\pi t/5)$

Amplitude (rad)	$A = 0.4$	$A = 0.6$	$A = 0.8$	$A = 1.0$	$A = 1.2$
PID	0.3377	0.3837	0.4317	0.4387	0.5870
NNLSMC	0.1231	0.1393	0.1491	0.2195	0.3302
NNTSMC	0.1145	0.1341	0.1393	0.1941	0.3700
ARFTNC	0.1094	0.1228	0.1318	0.1644	0.3288

the reference trajectory. The comparative results of the integrated absolute errors (IAE) are shown in Table 2. We can see from the table that the proposed ARFTNC method has the smallest IAE among all four control schemes. Compared with the NNLSMC, the NNTSMC achieves better tracking performance when $A = 0.4 \sim 1.0$, but for $A = 1.2$, its performance is deteriorated. PID controller gives the largest IAE in the all selected amplitude range (e.g., $A = 0.4 \sim 1.2$).

To display the comparison performance of tracking errors more intuitively, a reference example of $y_d = 1.0\sin(2\pi/5)$ is shown in Fig. 6. Figure 6a, b depicts the tracking errors and control signals, respectively. From Fig. 6, we can see that the proposed ARFTNC method performs better than other control schemes, which is consistent with the result given by Table 2.

5.3.3 *Example III: Tracking control of sinusoidal waves with varying frequencies*

In the following, we adopt a sinusoidal signal $y_d = 0.6\sin(2\pi/T)$ with a fixed amplitude but varying periods $T = 3.5 \sim 5.5$ s as the reference signal. Similar to the analysis of the second example, the tracking error performance in terms of IAE is provided by Table 3, and the comparative tracking errors and control signals for the reference $y_d = 0.6\sin(2\pi/4)$ are shown in Fig. 7a, b. From Table 3 and Fig. 7, we can see that the proposed ARFTNC can obtain faster convergence speed than NNTSMC and smaller tracking error than NNLSMC.

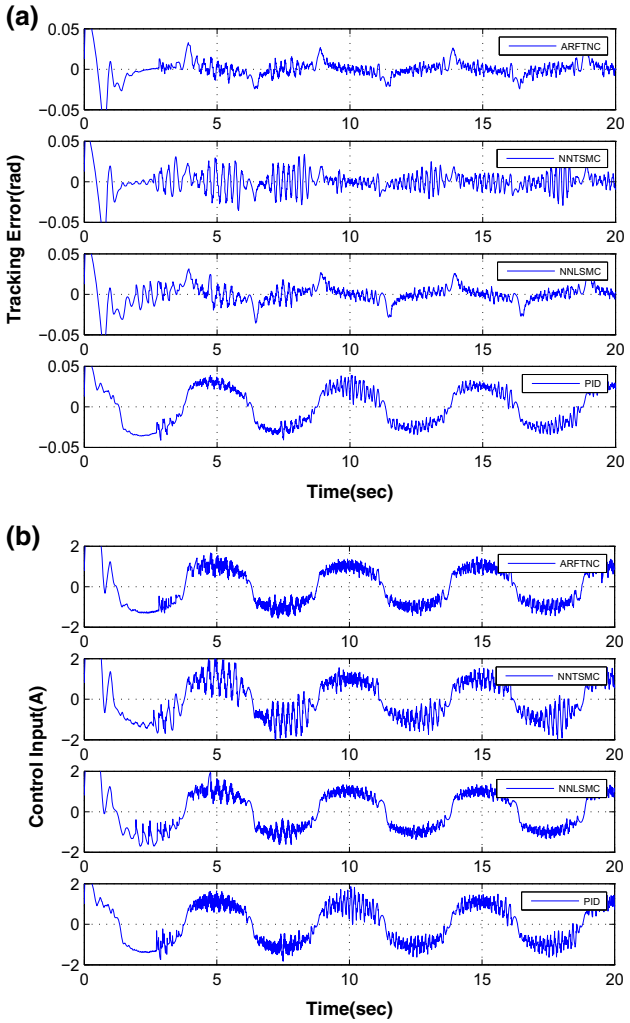

Fig. 6 Tracking control performance for $y_d = 1.0\sin(2\pi/5)$. **a** Tracking errors of four different controllers. **b** Control signals of four different controllers

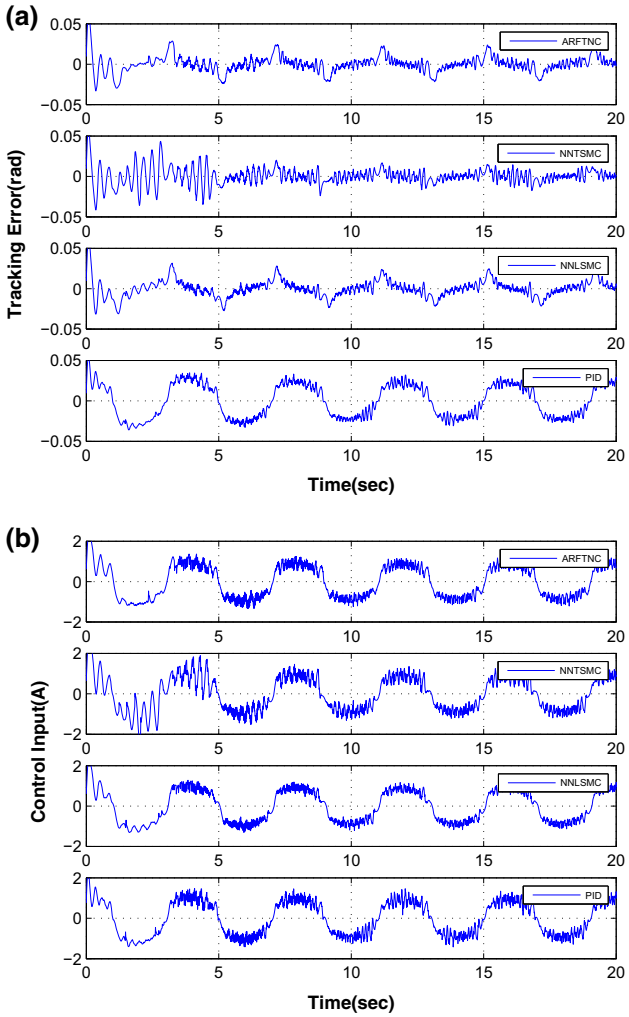

Fig. 7 Tracking control performance for $y_d = 0.6\sin(2\pi/4)$. **a** Tracking errors of four different controllers. **b** Control signals of four different controllers

Table 3 Tracking control performance IAE for $y_d = 0.6\sin(2\pi t/T)$

Period (s)	$T = 3.5$	$T = 4$	$T = 4.5$	$T = 5$	$T = 5.5$
PID	0.4133	0.4181	0.4001	0.3837	0.3570
NNLSMC	0.2019	0.1942	0.1453	0.1393	0.1338
NNTSMC	0.1727	0.1503	0.1323	0.1341	0.1199
ARFTNC	0.1614	0.1429	0.1256	0.1228	0.1169

5.3.4 *Example IV: Tracking control of sinusoidal waves with manual dead zone*

In order to further show the effect of dead zone and the control performance, we conduct extra experiments and compared their performance. For this purpose, a nonlinear dead zone is manually introduced before the control input $u(t)$ in the test-rig as shown in Fig. 4, and the expression is given as

$$u = \varphi(v) = \begin{cases} (1 - 0.3\sin(v))(v - 0.5) & u \leq -0.25 \\ 0 & -0.25 < v < 0.5 \\ (0.8 - 0.2\cos(v))(v + 0.25) & v \geq 0.5. \end{cases} \tag{55}$$

Then, three case studies are compared for the given sinusoidal signal $y_d = 0.6\sin(2\pi t/T)$:

Case 1: without dead zone (55)
Case 2: with dead zone (55) but no NN compensation
Case 3: with dead zone (55) and NN compensation

The tracking error comparison of the proposed ARFTNC for different cases is shown in Fig. 8. From Fig. 8, the following observations are obtained:

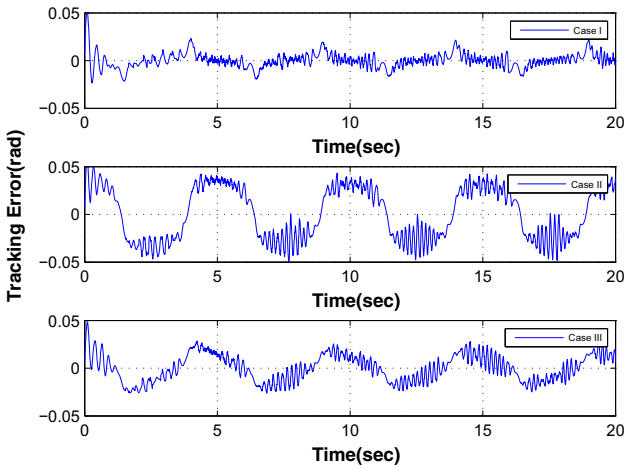

Fig. 8 Tracking errors comparison for different cases

(a) When the nonlinear dead zone (55) is introduced into test-rig, the tracking performance will be significantly deteriorated without any particular compensation.

(b) When the proposed adaptive NN compensation element is active, the tracking performance of ARFTNC scheme can be improved in the presence of the nonlinear dead zone perturbed in the system input.

This comparison exactly illustrates how the addition of the adaptive element allows for compensation of possible time-varying dynamics including the dead zone into the control design.

6 Conclusion

In this paper, we present an adaptive robust finite-time neural control scheme for uncertain PMSM servo system with nonlinear dead zone. The inverse compensation approach is avoided by representing the dead zone as a linear time-varying system. Based on a fast terminal sliding mode principle, the adaptive controller is designed by using a neural network as the nonlinearity estimator. In the proposed approach, the singularity problem is eliminated by modifying the TSMC manifold and the NN approximation error is compensated by employing a robust term. The boundedness of all signals and the finite-time stability of the closed-loop system are guaranteed based on the Lyapunov synthesis. Experimental results validate the improved tracking performance of the proposed method in comparison with several other controllers.

Acknowledgments The authors would thank the support from the National Natural Science Foundation of China under Grants Nos. 61403343, 61433003 and 61573174, and China Postdoctoral Science Foundation Funded Project under Grant No. 2015M580521.

References

1. Li SH, Liu Z (2009) Adaptive speed control for permanent-magnet synchronous motor system with variations of load inertia. IEEE Trans Ind Electron 56(8):3050–3059
2. Morawiec M (2013) The adaptive backstepping control of permanent magnet synchronous motor supplied by current source inverter. IEEE Trans Ind Inform 9(2):1047–1055
3. Liu G, Chen L, Zhao W et al (2013) Internal model control of permanent magnet synchronous motor using support vector machine generalized inverse. IEEE Trans Ind Inform 9(2):890–898
4. Tao G, Lewis FL (2001) Electric motor drives: modeling, analysis, and control. Springer, Berlin
5. Hu CX, Yao B, Wang QF (2011) Adaptive robust precision motion control of systems with unknown input dead-zones: a case study with comparative experiments. IEEE Trans Ind Electron 58(6):2454–2464
6. Han SI, Lee JM (2013) Precise positioning of nonsmooth dynamic systems using fuzzy wavelet echo state networks and dynamic surface sliding mode control. IEEE Trans Ind Electron 60(11):5124–5136
7. Xia D, Wang LY, Chai TY (2014) Neural-network friction compensation based energy swing-up control of pendubot. IEEE Trans Ind Electron 61(3):1411–1423
8. Naso D, Cupertino F, Turchiano B (2010) Precise position control of tubular linear motors with neural networks and composite learning. Control Eng Pract 18(5):515–522
9. Wang XS, Su CY, Hong H (2014) Robust adaptive control of a class of linear systems with unknown dead-zone. Automaica 40(3):407–413
10. Hua CC, Wang QG, Guan XP (2008) Adaptive tracking controller design of nonlinear systems with time delays and unknown dead-zone input. IEEE Trans Autom Control 53(7):1753–1759
11. Ibrir S, Xie WF, Su CY (2007) Adaptive tracking of nonlinear systems with non-symmetric dead-zone input. Automatica 43(3):522–530
12. Zhang TP, Ge SS (2007) Adaptive neural control of MIMO nonlinear state time-varying delay systems with unknown dead-zones and gain signs. Automatica 43(6):1021–1033
13. Zhang TP, Ge SS (2009) Adaptive neural network tracking control of MIMO nonlinear systems with unknown dead zones and control directions. IEEE Trans Neural Netw 20(3):483–497
14. Liu YJ, Zhou N (2010) Observer-based adaptive fuzzy-neural control for a class of uncertain nonlinear systems with unknown dead-zone input. ISA Trans 49(4):462–469
15. Na J, Ren XM, Herrmann G, Qiao Z (2011) Adaptive neural dynamic surface control for servo systems with unknown dead zone. Control Eng Pract 19(11):1328–1343
16. Man ZH, Paplinski AP, Wu HR (1994) A robust MIMO terminal sliding mode control scheme for rigid robotic manipulator. IEEE Trans Autom Control 39(12):2464–2469
17. Yu XH, Man ZH (2002) Fast terminal sliding-mode control design for nonlinear dynamical systems. IEEE Trans Circuits Syst I Fundam Theory Appl 49(2):261–264
18. Hong Y, Huang J, Xu Y (2001) On an output finite-time stabilization problem. IEEE Trans Autom Control 46(2):305–309
19. Feng Y, Yu XH, Man ZH (2002) Non-singular terminal sliding mode control of rigid manipulators. Automatica 38(12):2159–2167

20. Yu S, Yu XH, Shirinzadehc B (2005) Continuous finite-time control for robotic manipulators with terminal sliding mode. Automatica 41(11):1957–1964
21. Zhao DY, Li SY, Gao F (2009) A new terminal sliding mode control for robotic manipulators. Int J Control 82(10):1804–1813
22. Tang L, Liu YJ, Tong SC (2014) Adaptive neural control reinforcement learning for a class of robot manipulator. Neural Comput Appl 25:135–141
23. Na J, Chen Q, Ren XM, Guo Y (2014) Adaptive prescribed performance motion control of servo mechanisms with friction compensation. IEEE Trans Ind Electron 61(1):486–494
24. Na J, Ren XM, Zheng DD (2013) Adaptive control of nonlinear pure-feedback systems with high-order sliding mode observer. IEEE Trans Neural Netw Learn Syst 24(3):370–382
25. Wang LY, Chai TY, Zhai LF (2009) Neural-network-based terminal sliding-mode control of robotic manipulators including actuator dynamics. IEEE Trans Ind Electron 56(9):3296–3304
26. Zou AM, Kumar KD, Hou ZG, Liu X (2011) Finite-time attitude tracking control for spacecraft using terminal sliding mode and Chebyshev neural network. IEEE Trans Syst Man Cybern B Cybern 41(4):950–963
27. Lee MJ, Choi YK (2004) An adaptive neurocontroller using RBFNN for robot manipulators. IEEE Trans Ind Electron 51(3):711–717
28. Bhat SP, Bernstein DS (2000) Finite-time stability of continuous autonomous systems. SIAM J Control Optim 38(3):751–766